International Journal of Reconfigurable and Embedded Systems (IJRES)
Vol. 15, No. 1, March 2026, pp. 54~67
ISSN: 2089-4864, DOI: 10.11591/ijres.v15.i1.pp54-67

Online method for identifying Thevenin model parameters of Li-ion batteries and estimating SOC using EKF

Mouhssine Lagraoui[1], Ali Nejmi[1], Mouna Lhayani[2], Mohamed Benfars[3], Ahmed Abbou[2]
[1]Laboratory of Mathematics and Physics, Faculty of Sciences and Technics, Sultan Moulay Slimane University, Beni Mellal, Morocco
[2]Department of Electrical Engineering, Mohammadia School of Engineers, Mohammed V University in Rabat, Rabat, Morocco
[3]Laboratory of Industrial Engineering and Surface Engineering, Sultan Moulay Slimane University, Beni Mellal, Morocco

Article Info

Article history:

Received Jul 13, 2025
Revised Oct 21, 2025
Accepted Jan 11, 2026

Keywords:

Battery management system
Extended Kalman filter
Lithium-ion battery
State of charge
Thevenin model

ABSTRACT

Accurate state of charge (SOC) estimation is critical for the reliable operation of battery management systems (BMS) in electric vehicles (EVs) and energy storage applications. This paper presents a method for online identification of Thevenin model (TM) parameters and SOC estimation using the extended Kalman filter (EKF). The objective is to improve estimation accuracy by precisely characterizing the SOC-dependent variations of model parameters, including open-circuit voltage (V_{OCV}), internal resistance R_1, polarization resistance R_2, and capacitance C_2. These parameters are identified using least squares regression based on experimental discharge data from a 1.83 Ah lithium-ion (Li-ion) battery. The resulting model is validated under pulsed discharge conditions, achieving a mean absolute error (MAE) of 0.0059 V and root mean square error (RMSE) of 0.0074 V, indicating high modeling accuracy. Subsequently, an EKF algorithm is implemented using the identified model to estimate SOC in real time. Experimental results show excellent performance with an SOC estimation MAE of 0.059% and RMSE of 0.0798%, demonstrating high precision, fast convergence, and stability. The method effectively combines empirical parameter identification with a recursive filtering technique, offering a practical and embeddable solution for BMS applications. The study concludes that accurate parameter modeling significantly enhances EKF-based SOC estimation, providing a robust foundation for real-time battery monitoring and control.

Corresponding Author:

Mouhssine Lagraoui
Laboratory of Mathematics and Physics, Faculty of Sciences and Technics
Sultan Moulay Slimane University
Beni Mellal, Morocco
Email: mouhssine.lagraoui@gmail.com

1. INTRODUCTION

Accurate estimation of the state of charge (SOC) is a critical requirement for the reliable and efficient operation of battery management systems (BMS) in electric vehicles (EVs) and other energy-intensive applications. The SOC, which represents the available capacity of a lithium-ion battery as a percentage of its full charge, serves as a key indicator for energy management, safety monitoring, and longevity optimization. Inaccurate SOC estimation can lead to overcharging, deep discharging, reduced battery life, and even catastrophic failures. Therefore, developing robust, real-time, and high-precision SOC estimation methods remains a central challenge in modern battery technology.

Over the past few years, increasing energy demands and growing environmental concerns have accelerated the adoption of EVs, where lithium-ion batteries are the preferred energy storage solution due to their high energy density, lightweight, and long cycle life [1], [2]. Among the various parameters monitored by a BMS, the SOC is one of the most crucial, directly influencing vehicle range prediction, charging strategies, and overall system safety [3], [4]. Hence, precise SOC estimation not only enhances battery performance and lifespan but also ensures the safe and efficient operation of the entire system.

Several methodologies have been proposed in the literature to estimate the SOC of Li-ion batteries, each with distinct advantages and limitations. The coulomb counting method (CCM) is widely used due to its simplicity and ease of implementation. However, it is an open-loop algorithm that relies on accurate initial SOC and precise integration of current over time [5], [6]. In practice, sensor inaccuracies, current drift, and integration errors accumulate, leading to significant deviations in SOC estimation unless periodically corrected with other methods.

The open-circuit voltage (OCV) method exploits the direct correlation between the battery's OCV and its SOC. While highly accurate under resting conditions, this method requires prolonged idle periods to reach electrochemical equilibrium—making it unsuitable for real-time applications where continuous operation is demanded [7], [8].

To overcome the limitations of model-independent approaches, data-driven techniques such as neural networks (NN) and fuzzy logic (FL) have been explored. These intelligent algorithms can model complex nonlinear behaviors without requiring detailed knowledge of the internal battery dynamics [9]–[12]. However, they depend heavily on large, high-quality training datasets and substantial computational resources. Moreover, their generalization capability is limited when operating conditions differ from those in the training data, raising concerns about robustness and reliability.

Another promising approach is the particle filter (PF), which handles nonlinear and non-Gaussian systems effectively by representing the state distribution through stochastic particles [13], [14]. While flexible and powerful, the PF suffers from high computational complexity, particle degeneracy, and sample impoverishment—issues that make it less suitable for embedded systems with limited processing power.

In contrast, the Kalman filter (KF) and its variants offer a balanced solution by combining physical battery models with statistical estimation theory. The standard KF is optimal for linear systems but cannot be directly applied to the inherently nonlinear dynamics of Li-ion batteries. To address this, the extended Kalman filter (EKF) linearizes the system around the current operating point using first-order Taylor series expansions, enabling real-time state estimation with relatively low computational cost [15]–[18].

The EKF has gained widespread attention in SOC estimation, particularly when coupled with equivalent circuit models (ECMs) such as the Thevenin model (TM) [19]–[26]. This model effectively captures the dynamic voltage response of the battery using a combination of resistors and capacitors, along with an SOC-dependent OCV source. However, the accuracy of EKF-based estimation critically depends on the fidelity of the underlying model parameters—such as internal resistance, polarization resistance, and capacitance—all of which vary with SOC, temperature, and aging. Poor parameter identification leads to model mismatch, resulting in estimation bias and instability.

Despite extensive research, there remains a need for a systematic and accurate methodology to identify the SOC-dependent parameters of the TM and integrate them into an adaptive EKF framework for high-precision SOC estimation under dynamic operating conditions. This paper aims to address these challenges by proposing an online-capable method for simultaneous TM parameter identification and SOC estimation. The main contributions of this work are threefold:

- Precise parameter identification: using experimental discharge test data and least squares regression, we establish accurate functional relationships between the TM parameters (V_{OCV}, R_1, R_2, C_2) and SOC.
- Model validation: the identified model is rigorously validated against experimental pulsed discharge data, demonstrating high voltage prediction accuracy with a mean absolute error (MAE) of 0.0059 V and root mean square error (RMSE) of 0.0074 V.
- Robust SOC estimation: an EKF algorithm is designed based on the identified TM to estimate SOC in real time. Experimental results under constant-current pulsed discharge conditions show excellent performance, with an SOC estimation MAE of 0.059% and RMSE of 0.0798%, confirming the method's accuracy, fast convergence, and stability.

By integrating accurate parameter identification with an EKF-based estimation framework, this study provides a practical and effective solution for high-fidelity SOC estimation in Li-ion batteries, suitable for implementation in real-world BMS applications.

2. LI-ION BATTERY MODEL

2.1. The Thevenin model of a Li-ion battery

A precise battery modeling forms the basis for estimating the SOC of the battery. Battery models can be categorized into three types: electrochemical models (EM) [27], [28], mathematical models (MM) [29], and

ECM [30], [31]. The EM boasts high accuracy but has a complex structure that is challenging to implement, making it less suitable for battery modeling. While MM offer a simplified structure, they often fail to accurately represent the battery's external behavior. To maintain an optimal trade-off between model complexity and precision, this study employs a TM. The corresponding battery model schematic is presented in Figure 1.

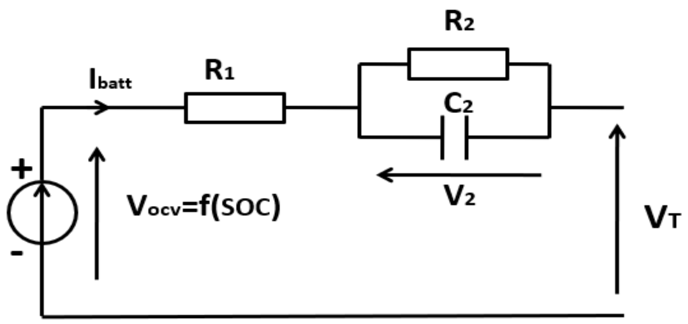

Figure 1. Circuit representation of the Thevenin-equivalent battery model

Figure 1 illustrates the TM where:
- Vocv denotes the OCV as a function of SOC
- Ibatt indicates the current flow through the battery
- V_T corresponds to the terminal voltage
- R_1 symbolizes the internal ohmic resistance
- The parallel combination of R_2 and C_2 characterizes the battery's polarization effects.
- V_2 reflects the potential difference across the polarization capacitance

The governing equations for this ECM can be derived as (1) and (2):

$$\begin{cases} \frac{dV_2}{dt} = -\frac{V_2}{R_2 C_2} + \frac{I_{batt}}{C_2} \\ \frac{dSOC}{dt} = -\frac{I_{batt}}{3600 \times AH} \end{cases} \tag{1}$$

$$V_T = V_{ocv}(SOC) - V_2 - R_{1\times} I_{batt} \tag{2}$$

Where AH: the battery capacity in A.h.

2.2. Parameter identification of the thevenin model

The TM parameters are identified through an approach that integrates theoretical modeling with experimental discharge measurements. This process entails optimizing the model's parameter values using empirical data to enhance the alignment between simulated outputs and experimental measurements. By refining this correlation, the model gains predictive capability for uncharacterized operational conditions.

This section presents the identification of the TM parameters through the analysis of in (1) and (2) and the battery discharge characteristics. The derived parameters include resistance R_1, the (R_2 and C_2) block, and the V_{OCV} (SOC) function.

The experimental study utilized a Li-ion battery cell with a rated capacity of 1.8 Ah. Testing involved a complete discharge cycle at 1C rate, after which the cell was allowed to rest for a minimum of two hours. The resulting voltage profile is illustrated in Figure 2(a), while the corresponding current discharge curve appears in Figure 2(b).

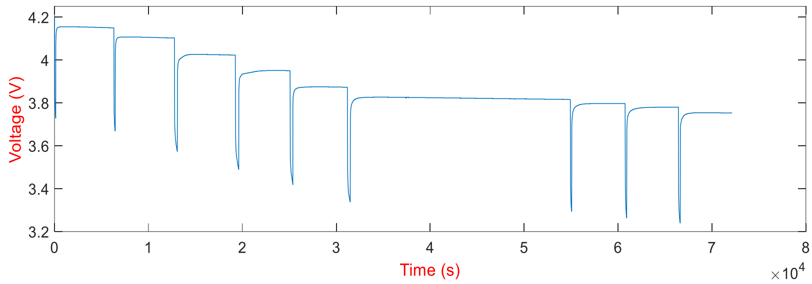

(a)

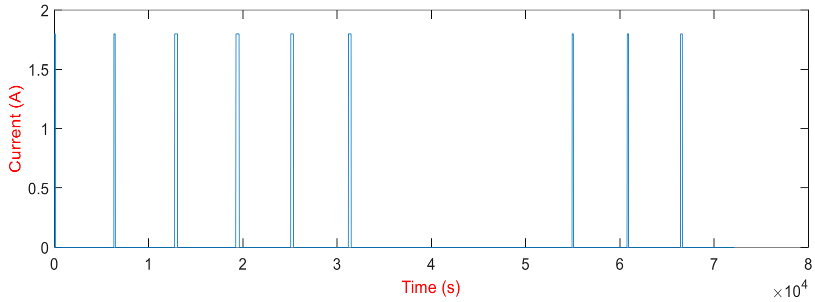

(b)

Figure 2. Presents the battery's discharge characteristics; (a) voltage profile during discharge and (b) applied current waveform

2.2.1. Identification of V_{ocv}-SOC relationship parameters

The correlation between SOC and V_{ocv} was established by analyzing voltage and SOC profiles generated through the CCM. The corresponding SOC-V_{ocv} data pairs are tabulated in Table 1.

Table 1. OCV-SOC correlation data

SOC	V_{OCV}	SOC	V_{OCV}
1	4.2	0.439	3.75
0.965	4.15	0.381	3.72
0.923	4.1	0.34	3.7
0.836	4.02	0.298	3.68
0.736	3.95	0.243	3.65
0.655	3.87	0.198	3.61
0.571	3.82	0.152	3.49
0.532	3.79	0.109	3.38
0.491	3.78	0.053	3.05

The MATLAB software was employed to establish the V_{ocv}-SOC correlation through least squares regression analysis of the dataset in Table 1. The resulting mathematical relationship $V_{ocv}=f(SOC)$ is expressed in (3), while Figure 3 displays the fitted characteristic curve between these parameters.

$$V_{ocv}(SOC) = k_1 + k_2 \times SOC + k_3 \times SOC^2 + k_4 \times SOC^3 + k_5 \times SOC^4 + k_6 \times SOC^5 \tag{3}$$

With $k_1 = 2.61, k_2 = 10.33, k_3 = -38.71, k_4 = 70.74, k_5 = -60.6 \textit{ and } k_6 = 19.84$

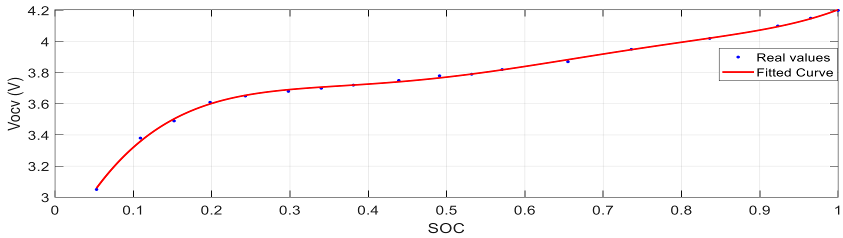

Figure 3. Fitting curve of the Vocv-SOC relationship

2.2.2. Identification of parameters R_1, R_2, and C_2 of the Thevenin model

To determine the variation of resistance R_1 depending on SOC, in this article, we used the voltage response curve of the battery's pulsed discharge. The discharge voltage diagram at a specific SOC value is depicted in Figure 4.

The part from V_a to V_b: the battery transitions from a resting state or SOC = 0.736 to a discharge state with a 1 C current, causing the battery terminal voltage to abruptly drop from the voltage potential V_a to potential V_b. According to the equivalent TM diagram, it's evident that V_2 cannot change abruptly. The sudden voltage drop from V_a to V_b is caused by the resistance R_1.

The voltage segment between V_c and V_d exhibits a sudden rise in battery terminal voltage following current interruption. This behavior mirrors the V_a-V_b transition and is attributable to the ohmic drop across internal resistance R_1. According to the parts from V_a to V_b and from V_c to V_d in Figure 4, the R_1 is obtained through the relationship:

$$R_1 = \frac{(V_a - V_b) + (V_d - V_c)}{2 * I_{batt}} = \frac{(3.95 - 3.6) + (3.767 - 3.419)}{2 * 1.8} = 0.1940\ \Omega \tag{4}$$

The relationship between SOC and R_1 was obtained by performing the same calculation as in (4) for each SOC value based on the discharge voltage curve, the equation $R_1(SOC)$ is presented in (4). Figure 5 depicts the curve of the fitted relationship between R_1 and SOC using the nonlinear least squares method employing MATLAB:

$$R_1(SOC) = a_1 + a_2 \times SOC + a_3 \times SOC^2 + a_4 \times SOC^3 + a_5 \times SOC^4 + a_6 \times SOC^5 \tag{5}$$

With $a_1 = 0.4139, a_2 = -1.689, a_3 = 6.352, a_4 = -11.92\ , a_5 = 10.56\ and\ a_6 = -3.528$

The potential range from V_d to V_e allows determining the values of R_2 and C_2. The diffusion resistance R_1 is determined from (6):

$$R_2 = \frac{V_e - V_d}{I_{batt}} = \frac{3.873 - 3.767}{1.799} = 0.059\ \Omega \tag{6}$$

The relationship between resistance R_2 and SOC was obtained by performing the same calculation as in (6) for each SOC value. The equation R_2=f(SOC) is presented in (7). Figure 6 depicts the curve of the fitted relationship between R_2 and SOC using the nonlinear least squares method with MATLAB.

$$R_2(SOC) = b_1 + b_2 \times SOC + b_3 \times SOC^2 + b_4 \times SOC^3 + b_5 \times SOC^4 + b_6 \times SOC^5 \tag{7}$$

With $b_1 = 0.5238, b_2 = -3.814, b_3 = 12.08, b_4 = -18.09, b_5 = 12.94\ and\ b_6 = -3.594$

To determine the time constant τ_2 for the part from V_d to V_e presented in the battery voltage discharge curve, we calculated the potential V_f, which represents the potential at time τ_2, using the following relationship:

$$V_f = V_d + 0.63 \times (V_e - V_d) = 3.833 + 0.63 \times (3.873 - 3.833) = 3.858\ \text{V} \tag{8}$$

Based on the potential V_f, we deduce τ_2:

$$\tau_2 = 25430 - 25380 = 50\ \text{s} \tag{9}$$

Therefore, the diffusion capacity C_2 is calculated as (10):

$$C_2 = \frac{\tau_2}{R_2} = \frac{50}{0.059} = 847.46\ F \tag{10}$$

By using the same calculation procedure for each SOC value, the relationship between the capacity C_2 and SOC was established. The equation C_2=f(SOC) is presented in (11). Figure 7 shows the curve of the fitted relationship between C_2 and SOC using the nonlinear least squares method with MATLAB.

$$C_2(SOC) = c_1 + c_2 \times SOC + c_3 \times SOC^2 + c_4 \times SOC^3 + c_5 \times SOC^4 + c_6 \times SOC^5 + c_7 \times SOC^6 + +c_8 \times SOC^7 \tag{11}$$

With $c_1 = 202.7, c_2 = 9245, c_3 = -9.637 \times 10^4, c_4 = 5.04 \times 10^5, c_5 = -1.262 \times 10^6, c_6 = 1.598 \times 10^6, c_7 = -9.972 \times 10^5$ *and* $c_8 = 2.446 \times 10^5$

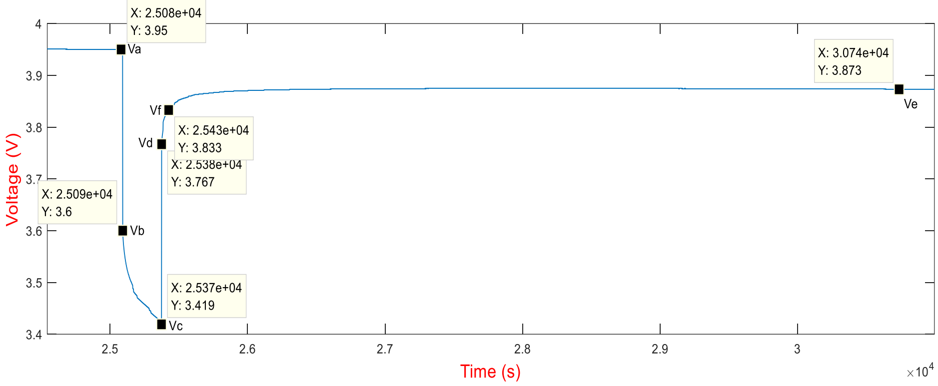

Figure 4. An enlarged section of the discharge voltage curve corresponding to a SOC of 0.655

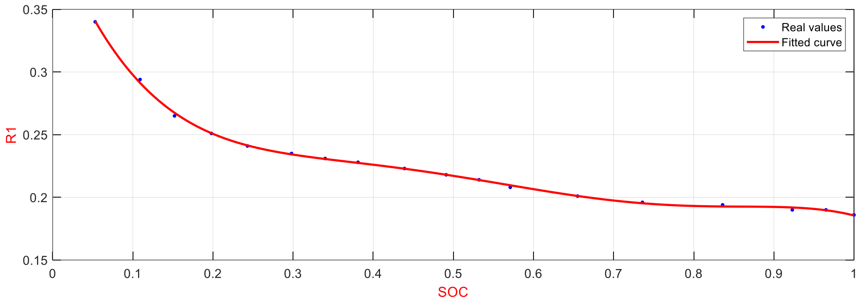

Figure 5. Fitting curve of the R_1-SOC relationship

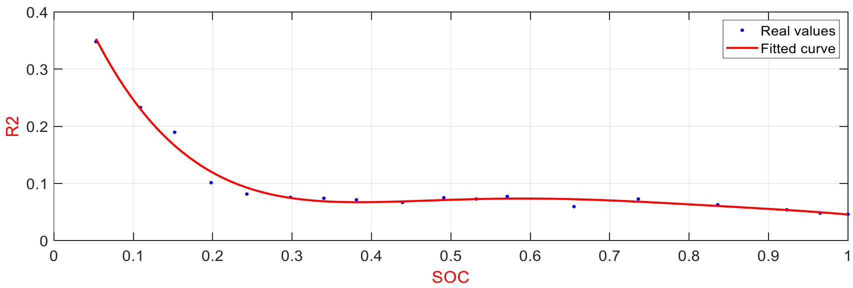

Figure 6. Fitting curve of the R_2-SOC relationship

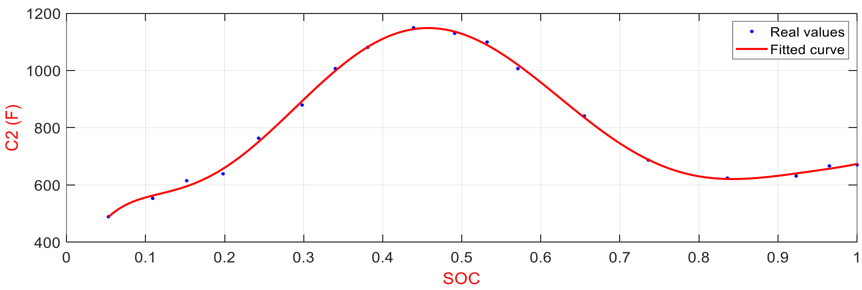

Figure 7. Fitting curve of the C_2-SOC relationship

3. SOC ESTIMATION FOR BATTERIES USING EKF

As a nonlinear system, the battery's behavior is described by state and observation equations that account for both process noise and measurement noise. These governing equations are mathematically expressed in (12) and (13):

$$x_{k+1} = f(x_k, u_k) + w \tag{12}$$

$$y_k = h(x_k, u_k) + v \tag{13}$$

In these expressions, the discrete time index k indicates the present timestep. The nonlinear state transition function $f(x_k, u_k)$ describes the system dynamics, while $h(x_k, u_k)$ models the measurement relationships. Here, x_k corresponds to the system state vector, u_k to the control input, and y_k to the measurable output. The terms w and v respectively characterize the process disturbance and measurement uncertainty inherent in the system.

As depicted in (12) and (13), we are assuming that both functions are differentiable at every operating point.

$$f(x_k, u_k) \approx f(\hat{x}_{k-1}, u_k) + \frac{\partial f(x_k,u_k)}{\partial x_k}\bigg|_{x_k=\hat{x}_{k-1}} (x_k - \hat{x}_{k-1}) \tag{14}$$

$$h(x_k, u_k) \approx h(\hat{x}_k^-, u_k) + \frac{\partial h(x_k,u_k)}{\partial x_k}\bigg|_{x_k=\hat{x}_k^-} (x_k - \hat{x}_k^-) \tag{15}$$

By substituting in (14) and (15) into in (12) and (13), the linearized process and measurement models transform into:

$$x_{k+1} \approx \hat{A}_k x_k + f(\hat{x}_{k-1}, u_k) - \hat{A}_k \hat{x}_{k-1} + w \tag{16}$$

$$h(x_k, u_k) \approx \widehat{H}_k x_k + h(\hat{x}_k^-, u_k) - \widehat{H}_k \hat{x}_k^- + v \tag{17}$$

We define $\hat{A}_k$ and $\widehat{H}_k$in the following manner:

$$\hat{A}_k = \frac{\partial f(x_k,u_k)}{\partial x_k}\bigg|_{x_k=\hat{x}_{k-1}} \tag{18}$$

$$\widehat{H}_k = \frac{\partial h(x_k,u_k)}{\partial x_k}\bigg|_{x_k=\hat{x}_k^-} \tag{19}$$

$$x_k = \begin{bmatrix} SOC \\ V_2 \end{bmatrix} = \begin{bmatrix} x_1 \\ x_2 \end{bmatrix} \tag{20}$$

$$u_k = I_{batt} \tag{21}$$

$$y_k = V_{batt} \tag{22}$$

Where x_k is the system state vector at the sampling time k, I_{batt} is the battery current, and V_{batt} is the battery voltage.

The state transition equations are established through discretization and linearization of both the TM's mathematical relationships and the current integration method formulation, as presented:

$$f(x_k, u_k) = \begin{bmatrix} f_1 \\ f_2 \end{bmatrix} \tag{23}$$

$$f_1 = SOC(k-1) - \frac{\Delta t}{3600.AH} \times I_{batt}(k) \tag{24}$$

$$f_1 = x_1 - \frac{\Delta t}{3600.AH} \times u \tag{25}$$

$$f_2 = V_2(k-1) \times e^{-\frac{\Delta t}{R_2(SOC).C_2(SOC)}} - R_2(SOC)\,(1 - e^{-\frac{\Delta t}{R_2(SOC).C_2(SOC)}}) \times I_{batt}(k) \tag{26}$$

$$f_2 = x_2 \times e^{-\frac{\Delta t}{R_2(x_1)C_2(x_1)}} - R_2\,(x_1)(1 - e^{-\frac{\Delta t}{R_2(x_1)C_2(x_1)}}) \times u(k) \tag{27}$$

$$h(x_k, u_k) \ = V_{ocv}(SOC) - V_1 - R_1(SOC) \times I_{batt}(k) \tag{28}$$

$$h(x_k, u_k) = V_{ocv}(x_1) - x_2 - R_1(x_1) \times u(k) \tag{29}$$

We need to compute the two Jacobians, A and H, in order to use this model in the EKF algorithm. Consequently, the derivative of the function f and function h with respect to the state variables is as (30) and (31):

$$\hat{A}_k = \frac{\partial f(x_k,u_k)}{\partial x_k}\bigg|_{x_k=\hat{x}_{k-1}} = \begin{pmatrix} F_{11} & F_{12} \\ F_{21} & F_{22} \end{pmatrix} \tag{30}$$

$$\widehat{H}_k = \frac{\partial h(x_k,u_k)}{\partial x_k}\bigg|_{x_k=\hat{x}_k^-} = (H_1 \quad H_2) \tag{31}$$

After calculating the various partial derivatives of function f, we obtain the following results:

$$F_{11} = 1, F_{12} = 0 \tag{32}$$

$$F_{21} = [(b_2 + 2b_3x_1 + 3b_4x_1^2 + 4b_5x_1^3 + 5b_6x_1^4) \times u(k) \times (e^{-\frac{\Delta t}{R_2C_2}} - 1)] - [(x_2 + R_2 \times u(k)) \times \Delta t \times \frac{(b_2+2b_3x_1+3b_4x_1^2+4b_5x_1^3+5b_6x_1^4)\times C_2+R_2\times(c_2+2c_3x_1+3c_4x_1^2+4c_5x_1^3+5c_6x_1^4+6c_7x_1^5+7c_8x_1^6)}{(R_2C_2)^2} \times e^{-\frac{\Delta t}{R_2C_2}}] \tag{33}$$

and $F_{22} = e^{-\frac{\Delta t}{R_2C_2}}$ (34)

After calculating the various partial derivatives of function h, we get the results:

$$H_1 = k_2 + 2k_3 \times SOC + 3k_4 \times SOC^2 + 4k_5 \times SOC^3 + 5k_6 \times SOC^4 \tag{35}$$

$$H_2 = -1 \tag{36}$$

Figure 8 illustrates the sequential stages of the EKF computational process.

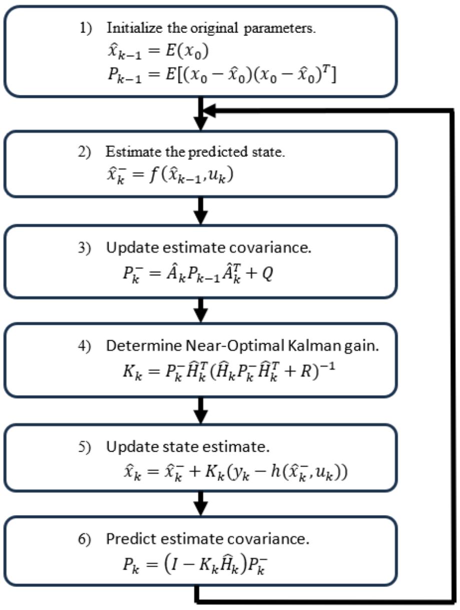

Figure 8. Sequential operations in the EKF recursive estimation process

4. EXPERIMENTAL RESULTS AND DISCUSSION

This section presents and discusses the key findings of the proposed method for TM parameter identification and SOC estimation using the EKF. The experimental validation focuses on two primary aspects: i) the accuracy of the identified battery model in predicting terminal voltage, and ii) the performance of the EKF in estimating the SOC under dynamic discharge conditions.

4.1. Model validation results

The TM parameters—open-circuit voltage (V_{OCV}, internal resistance R_1, polarization resistance R_2, and capacitance C_2 —were identified as functions of SOC using least squares regression on experimental discharge data. These SOC-dependent functions were then integrated into the model to simulate the battery's terminal voltage response under pulsed discharge conditions.

Figure 9 shows a close match between the simulated and experimentally measured terminal voltages, indicating that the identified model accurately captures the dynamic behavior of the battery. The modeling error, depicted in Figure 10, remains within ±0.038 V across the entire discharge cycle, with no significant systematic deviation.

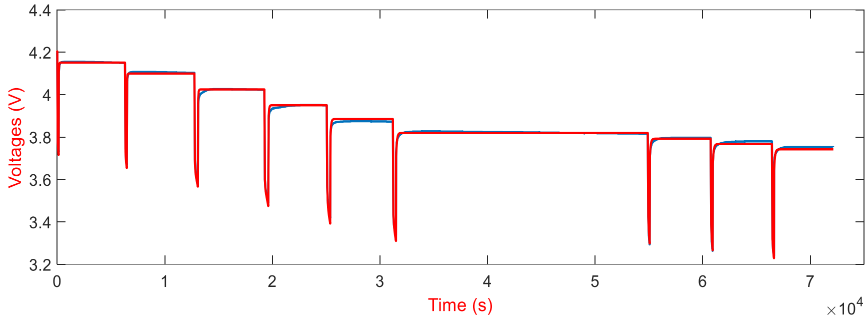

Figure 9. Comparison between simulated terminal voltage and experimentally measured battery voltage

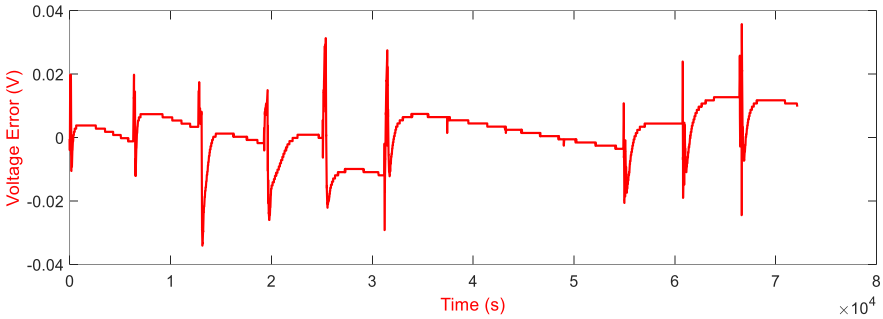

Figure 10. The modeling error of the voltage at the battery terminals

The quantitative assessment of model accuracy is summarized in Table 2, which reports a MAE of 0.0057 V and a RMSE of 0.0074 V. These low error values confirm the high fidelity of the parameter identification process and the effectiveness of the TM in representing the battery's electrical dynamics.

Table 2. Voltage modeling error metrics

Type of error	MAE	RMSE
Value	0.0057	0.0074

This level of accuracy is comparable to or better than results reported in similar studies. For instance, Plett [22] achieved a voltage RMSE of approximately 0.01 V using a comparable ECM-based approach, while He *et al*. [25] reported an RMSE of 0.0085 V with an improved TM. The superior performance of our model can be attributed to the precise, experimentally derived SOC-dependent parameter functions, particularly the high-resolution OCV-SOC relationship established via polynomial fitting.

4.2. State of charge estimation performance

The EKF algorithm was implemented using the identified TM to estimate the SOC in real time. The initial SOC was set to 1 (fully charged), and the filter was validated under constant-current pulsed discharge conditions. The reference SOC was computed using the CCM, which, although prone to drift over time, provides a reliable benchmark over short to medium durations when properly initialized.

$$x_0 = \begin{bmatrix} 1 \\ 0.1 \end{bmatrix}, P_0 = \begin{bmatrix} 10^{-8} & 0 \\ 0 & 10^{-8} \end{bmatrix}, Q = \begin{bmatrix} 10^{-6} & 0 \\ 0 & 10^{-6} \end{bmatrix} \text{ and } R = 10000$$

Figure 11 shows the device used to conduct the battery discharge and charge test. The cell utilized in this test is a Li-ion type cell with an actual capacity of 1.8 AH. The battery discharge test is employed to verify the accuracy of the TM and the EKF.

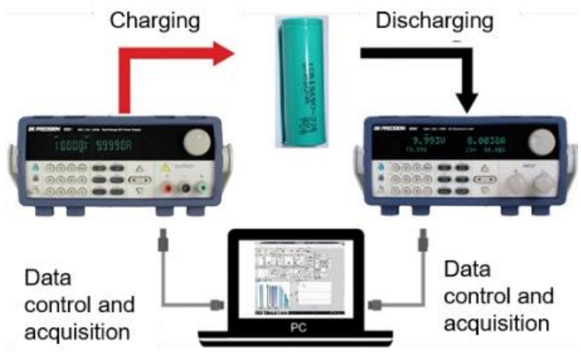

Figure 11. The schematic of the battery discharge and charging device

Figure 12(a) (see subsection 4.3) shows that the EKF-estimated SOC closely follows the reference trajectory, demonstrating fast convergence and minimal steady-state deviation. The maximum estimation error does not exceed 0.15%, as shown in Figure 12(b) (see subsection 4.3), and the error quickly settles after transient events such as current pulses.

The overall estimation accuracy is quantified in Table 3, which reports an MAE of 0.059% and an RMSE of 0.0798%—indicating exceptional precision. These results surpass the performance reported in several recent studies. For example, Mawonou *et al*. [16] achieved an SOC RMSE of 0.3% using a fractional-order EKF, while Tian *et al*. [18] reported an RMSE of 0.15% using a hybrid LSTM-Kalman approach. The superior accuracy of our method is primarily due to the high-fidelity parameter identification process, which minimizes model-plant mismatch—a known source of estimation bias in EKF-based methods. To evaluate the robustness of our approach, Figure 13 (see subsection 4.3) shows that the SOC estimation converges across varying initial SOC values (SOC_0 = 0.1, 0.3, 0.5, 0.7, and 0.9).

4.3. Interpretation and comparison with existing work

The strong agreement between estimated and reference SOC values confirms that the proposed method successfully achieves its primary objective: accurate, real-time SOC estimation through precise modeling and effective filtering. By rigorously identifying the SOC-dependency of all key model parameters, the method reduces reliance on heuristic assumptions and enhances the EKF's ability to track true SOC under dynamic conditions.

Compared to data-driven approaches such as NNs [9]–[12], the proposed method requires less computational power and avoids the need for large training datasets. Unlike the PF [13], [14] it maintains low computational complexity, making it suitable for embedded BMS applications. Furthermore, the use of a physically interpretable ECM enhances transparency and facilitates integration with other BMS functions such as health monitoring and fault detection.

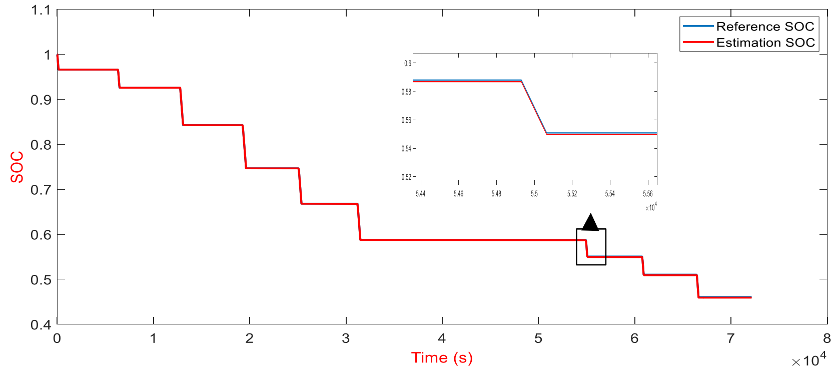

(a)

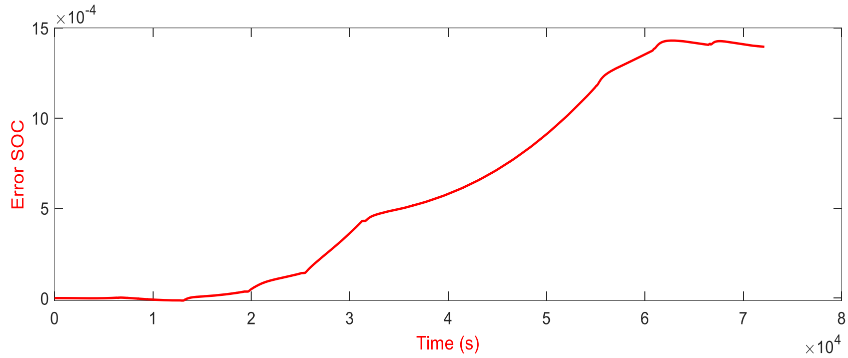

(b)

Figure 12. SOC estimation; (a) estimated values and (b) estimation error

Table 3. The SOC estimation error metrics

Type of error	MAE %	RMSE%
Value	0.059	0.0798

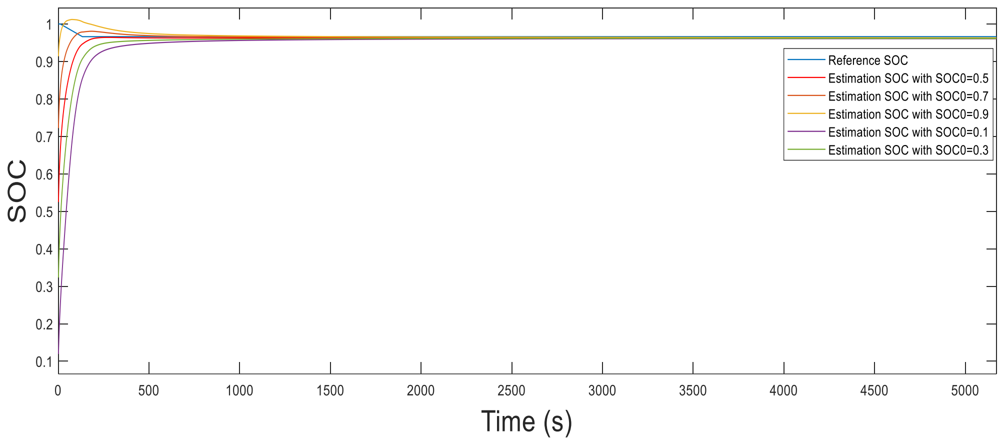

Figure 13. SOC estimation results when the initial SOC is unknown

4.4. Limitations and future work

Despite its high accuracy, this study has several limitations. First, the parameter identification was performed at room temperature and under a single discharge rate (1C), which may limit the model's generalization to varying temperatures and load profiles. Battery parameters are known to be temperature- and aging-dependent, and future work will extend the identification process to include these effects.

Second, while the EKF handles mild nonlinearities effectively, higher-order filters such as the unscented Kalman filter (UKF) or adaptive EKF variants could potentially improve robustness under more extreme operating conditions.

Finally, the current validation is based on laboratory-scale experiments. Real-world validation on vehicle drive cycles and integration into a hardware-in-the-loop (HIL) BMS platform will be pursued in future work. Nonetheless, the results demonstrate that the proposed online parameter identification and EKF-based SOC estimation framework is highly accurate, stable, and suitable for practical implementation in lithium-ion BMSs.

5. CONCLUSION

This study employed least squares regression to determine SOC-dependent parameter variations in the battery model using experimental discharge data. The methodology successfully established the fundamental V_{OCV}-SOC correlation critical for accurate modeling. Model verification through MATLAB simulations demonstrated exceptional voltage prediction capability, with validation tests yielding a MAE of 0.0059 V and RMSE of 0.0074 V, confirming the model's high precision.

The implemented Thevenin-based EKF algorithm achieved robust SOC estimation performance during constant-current pulsed discharge experiments. Comparative analysis with reference measurements revealed outstanding estimation accuracy (MAE: 0.059% and RMSE: 0.0798%), along with rapid convergence and stable performance characteristics. These results validate the effectiveness of combining precise, experimentally derived parameter identification with the EKF framework for high-fidelity SOC estimation.

In summary, this research presents a practical, accurate, and computationally efficient solution for SOC estimation in lithium-ion batteries. By integrating rigorous experimental parameter identification with a robust EKF framework, the study advances the state of the art in BMS design and paves the way for smarter, safer, and more sustainable energy storage technologies.

FUNDING INFORMATION

Authors state no funding involved.

AUTHOR CONTRIBUTIONS STATEMENT

This journal uses the Contributor Roles Taxonomy (CRediT) to recognize individual author contributions, reduce authorship disputes, and facilitate collaboration.

Name of Author	C	M	So	Va	Fo	I	R	D	O	E	Vi	Su	P	Fu
Mouhssine Lagraoui	✓	✓	✓	✓	✓	✓	✓	✓	✓	✓				✓
Ali Nejmi		✓				✓	✓			✓	✓	✓		
Mouna Lhayani		✓					✓		✓					
Mohamed Benfars					✓		✓			✓				
Ahmed Abbou						✓	✓			✓				

C : **C**onceptualization
M : **M**ethodology
So : **So**ftware
Va : **Va**lidation
Fo : **Fo**rmal analysis
I : **I**nvestigation
R : **R**esources
D : **D**ata Curation
O : Writing - **O**riginal Draft
E : Writing - Review & **E**diting
Vi : **Vi**sualization
Su : **Su**pervision
P : **P**roject administration
Fu : **Fu**nding acquisition

CONFLICT OF INTEREST STATEMENT

Authors state no conflict of interest.

DATA AVAILABILITY

The data that support the findings of this study are available from the corresponding author (M.L.) upon reasonable request.

REFERENCES

[1] G. Gruosso, G. S. Gajani, F. Ruiz, J. D. Valladolid, and D. Patino, "A virtual sensor for electric vehicles' state of charge estimation," *Electronics (Switzerland)*, vol. 9, no. 2, p. 278, Feb. 2020, doi: 10.3390/electronics9020278.

[2] Y. Yang, Z. Tan, and Y. Ren, "Research on factors that influence the fast-charging behavior of private battery electric vehicles," *Sustainability (Switzerland)*, vol. 12, no. 8, 2020, doi: 10.3390/SU12083439.

[3] F. Feng *et al.*, "Co-estimation of lithium-ion battery state of charge and state of temperature based on a hybrid electrochemical-thermal-neural-network model," *Journal of Power Sources*, vol. 455, 2020, doi: 10.1016/j.jpowsour.2020.227935.

[4] Y. Li, P. Chattopadhyay, S. Xiong, A. Ray, and C. D. Rahn, "Dynamic data-driven and model-based recursive analysis for estimation of battery state-of-charge," *Applied Energy*, vol. 184, pp. 266–275, 2016, doi: 10.1016/j.apenergy.2016.10.025.

[5] K. S. Ng, C. S. Moo, Y. P. Chen, and Y. C. Hsieh, "Enhanced coulomb counting method for estimating state-of-charge and state-of-health of lithium-ion batteries," *Applied Energy*, vol. 86, no. 9, pp. 1506–1511, 2009, doi: 10.1016/j.apenergy.2008.11.021.

[6] C. Lin, Q. Chen, J. Wang, W. Huang, and Y. Wang, "Improved Ah counting method for state of charge estimation of electric vehicle batteries," *Qinghua Daxue Xuebao/Journal of Tsinghua University*, vol. 46, no. 2, pp. 247–251, 2006.

[7] X. Chen, H. Lei, R. Xiong, W. Shen, and R. Yang, "A novel approach to reconstruct open circuit voltage for state of charge estimation of lithium ion batteries in electric vehicles," *Applied Energy*, vol. 255, 2019, doi: 10.1016/j.apenergy.2019.113758.

[8] C. Stolze, M. D. Hager, and U. S. Schubert, "State-of-charge monitoring for redox flow batteries: A symmetric open-circuit cell approach," *Journal of Power Sources*, vol. 423, pp. 60–67, 2019, doi: 10.1016/j.jpowsour.2019.03.002.

[9] M. S. H. Lipu, M. A. Hannan, A. Hussain, and M. H. M. Saad, "Optimal BP neural network algorithm for state of charge estimation of lithium-ion battery using PSO with PCA feature selection," *Journal of Renewable and Sustainable Energy*, vol. 9, no. 6, 2017, doi: 10.1063/1.5008491.

[10] Z. Li, D. Liu, F. Lu, X. Heng, Y. Guo, and Q. Jiang, "Research on SOC estimation of lithium battery based on GWO-BP neural network," *Proceedings of the 15th IEEE Conference on Industrial Electronics and Applications, ICIEA 2020*, 2020, pp. 506–510, doi: 10.1109/ICIEA48937.2020.9248364.

[11] F. Yang, W. Li, C. Li, and Q. Miao, "State-of-charge estimation of lithium-ion batteries based on gated recurrent neural network," *Energy*, vol. 175, pp. 66–75, 2019, doi: 10.1016/j.energy.2019.03.059.

[12] C. Bian, H. He, and S. Yang, "Stacked bidirectional long short-term memory networks for state-of-charge estimation of lithium-ion batteries," *Energy*, vol. 191, 2020, doi: 10.1016/j.energy.2019.116538.

[13] L. Martino, J. Read, V. Elvira, and F. Louzada, "Cooperative parallel particle filters for online model selection and applications to urban mobility," *Digital Signal Processing: A Review Journal*, vol. 60, pp. 172–185, 2017, doi: 10.1016/j.dsp.2016.09.011.

[14] L. Martino, V. Elvira, and G. Camps-Valls, "Group Importance Sampling for particle filtering and MCMC," *Digital Signal Processing: A Review Journal*, vol. 82, pp. 133–151, 2018, doi: 10.1016/j.dsp.2018.07.007.

[15] M. Lagraoui, S. Doubabi, and A. Rachid, "SOC estimation of Lithium-ion battery using Kalman filter and Luenberger observer: A comparative study," *Proceedings of 2014 International Renewable and Sustainable Energy Conference, IRSEC 2014*, 2014, pp. 636–641, doi: 10.1109/IRSEC.2014.7059849.

[16] K. S. R. Mawonou, A. Eddahech, D. Dumur, D. Beauvois, and E. Godoy, "Improved state of charge estimation for Li-ion batteries using fractional order extended Kalman filter," *Journal of Power Sources*, vol. 435, 2019, doi: 10.1016/j.jpowsour.2019.226710.

[17] F. Guo, G. Hu, S. Xiang, P. Zhou, R. Hong, and N. Xiong, "A multi-scale parameter adaptive method for state of charge and parameter estimation of lithium-ion batteries using dual Kalman filters," *Energy*, vol. 178, pp. 79–88, 2019, doi: 10.1016/j.energy.2019.04.126.

[18] Y. Tian, R. Lai, X. Li, L. Xiang, and J. Tian, "A combined method for state-of-charge estimation for lithium-ion batteries using a long short-term memory network and an adaptive cubature Kalman filter," *Applied Energy*, vol. 265, 2020, doi: 10.1016/j.apenergy.2020.114789.

[19] M. Partovibakhsh and G. Liu, "An adaptive unscented kalman filtering approach for online estimation of model parameters and state-of-charge of lithium-ion batteries for autonomous mobile robots," *IEEE Transactions on Control Systems Technology*, vol. 23, no. 1, pp. 357–363, 2015, doi: 10.1109/TCST.2014.2317781.

[20] S. Wang, C. Fernandez, C. Yu, Y. Fan, W. Cao, and D. I. Stroe, "A novel charged state prediction method of the lithium ion battery packs based on the composite equivalent modeling and improved splice Kalman filtering algorithm," *Journal of Power Sources*, vol. 471, 2020, doi: 10.1016/j.jpowsour.2020.228450.

[21] M. Lagraoui, A. Nejmi, H. Rayhane, and A. Taouni, "Estimation of lithium-ion battery state-of-charge using an extended kalman filter," *Bulletin of Electrical Engineering and Informatics*, vol. 10, no. 4, pp. 1759–1768, 2021, doi: 10.11591/eei.v10i4.3082.

[22] G. L. Plett, "Extended Kalman filtering for battery management systems of LiPB-based HEV battery packs - Part 2. Modeling and identification," *Journal of Power Sources*, vol. 134, no. 2, pp. 262–276, 2004, doi: 10.1016/j.jpowsour.2004.02.032.

[23] G. L. Plett, "Extended Kalman filtering for battery management systems of LiPB-based HEV battery packs - Part 3. State and parameter estimation," *Journal of Power Sources*, vol. 134, no. 2, pp. 277–292, 2004, doi: 10.1016/j.jpowsour.2004.02.033.

[24] G. L. Plett, "Extended Kalman filtering for battery management systems of LiPB-based HEV battery packs - Part 1. Background," *Journal of Power Sources*, vol. 134, no. 2, pp. 252–261, 2004, doi: 10.1016/j.jpowsour.2004.02.031.

[25] H. He, R. Xiong, X. Zhang, F. Sun, and J. Fan, "State-of-charge estimation of the lithium-ion battery using an adaptive extended Kalman filter based on an improved Thevenin model," *IEEE Transactions on Vehicular Technology*, vol. 60, no. 4, pp. 1461–1469, 2011, doi: 10.1109/TVT.2011.2132812.

[26] M. Lagraoui and A. Nejmi, "Estimation of Lithium-Ion Battery State-of-Charge Using an Unscented Kalman Filter," *Lecture Notes in Electrical Engineering*, vol. 1141, pp. 678–689, 2024, doi: 10.1007/978-981-97-0126-1_60.

[27] C. Lin, A. Tang, and J. Xing, "Evaluation of electrochemical models based battery state-of-charge estimation approaches for electric vehicles," *Applied Energy*, vol. 207, pp. 394–404, 2017, doi: 10.1016/j.apenergy.2017.05.109.

[28] F. Ringbeck, M. Garbade, and D. U. Sauer, "Uncertainty-aware state estimation for electrochemical model-based fast charging control of lithium-ion batteries," *Journal of Power Sources*, vol. 470, 2020, doi: 10.1016/j.jpowsour.2020.228221.

[29] A. Seaman, T. S. Dao, and J. McPhee, "A survey of mathematics-based equivalent-circuit and electrochemical battery models for hybrid and electric vehicle simulation," *Journal of Power Sources*, vol. 256, pp. 410–423, 2014, doi: 10.1016/j.jpowsour.2014.01.057.

[30] X. Zhang, J. Lu, S. Yuan, J. Yang, and X. Zhou, "A novel method for identification of lithium-ion battery equivalent circuit model parameters considering electrochemical properties," *Journal of Power Sources*, vol. 345, pp. 21–29, 2017, doi: 10.1016/j.jpowsour.2017.01.126.

[31] A. Bhattacharjee, A. Roy, N. Banerjee, S. Patra, and H. Saha, "Precision dynamic equivalent circuit model of a Vanadium Redox Flow Battery and determination of circuit parameters for its optimal performance in renewable energy applications," *Journal of Power Sources*, vol. 396, pp. 506–518, 2018, doi: 10.1016/j.jpowsour.2018.06.017.

BIOGRAPHIES OF AUTHORS

Mouhssine Lagraoui received his diploma in Electrical Engineer from National School of Applied Sciences ENSA Marrakech, Morrocco, in 2012. He is currently a postgraduate student pursuing his doctorate's degree under the supervision of Dr Ali Nejmi in Laboratory of Mathematics and Physics, Faculty of Sciences and Technics, Beni Mellal, Morrocco. His research concerns with battery management system (BMS). He can be contacted at email: mouhssine.lagraoui@gmail.com.

Ali Nejmi received his diploma in Electrical Engineer and Advanced Graduate Studies degree from Mohammadia School of Engineers, Morocco, in 1995 and 2001, respectively. He received his doctorate degree from Sultan Moulay Slimane University, Morocco, in 2015. He has been an associate professor at the Department of Electrical, Faculty of Sciences and Technics, Sultan Moulay Slimane University, Morocco, since 1996. His field of research interest includes nonlinear control of electrical machines, renewable energies plants integration in electrical grids, and hybrid micro-grids. He can be contacted at email: ali.nejmi@gmail.com.

Mouna Lhayani received her Master's degree in renewable energies and storage from the Faculty of Science in Rabat, Morocco, in 2018. Currently, she is a postgraduate student pursuing her doctorate under the supervision of Dr. Ahmed Abbou at the Mohammadia School of Engineers in Rabat, Morocco. Her research focuses on the trajectory control of quadrotor systems. She can be contacted at email: mounalhayani@research.emi.ac.ma.

Mohamed Benfars obtained his specialized master's degree in Energy Engineering and Environment from the Faculty of Sciences in Tetouan, Morocco, in 2020. He is currently a graduate student pursuing his Ph.D. under the supervision of Professor Mustapha Mabrouki at the Laboratory of Industrial Engineering and Surface Engineering, Faculty of Sciences and Techniques, Beni Mellal, Morocco. He can be contacted at email: benfars.mohammed@usmc.ac.ma.

Ahmed Abbou received the B.E. degree from ENSET in Rabat, the M.E. degree from Mohammed V University in Rabat and the Ph.D. degree from Mohammed V University in Rabat, in 2000, 2005 and 2009, respectively, all in electrical engineering. Since 2009, he has been working at Mohammadia School of engineers, Mohammed V University in Rabat, Department of electric Power Engineering, where he is a full Professor of Power Electronics and Electric drives. He published numerous papers in scientific international journals and conferences proceedings. His current research interests include induction machine control systems, self-excited induction generator, power electronics, sensorless drives for AC machines, and renewable energy (PV and wind energy). He can be contacted at email: abbou_a@yahoo.fr.